

Studies of spin-orbit scattering in noble-metal nanoparticles using energy level tunneling spectroscopy

J. R. Petta and D. C. Ralph

Laboratory of Atomic and Solid State Physics, Cornell University, Ithaca, New York 14853

(October 30, 2018)

The effects of spin-orbit scattering on discrete electronic energy levels are studied in copper, silver, and gold nanoparticles. Level-to-level fluctuations of the effective g -factor for Zeeman splitting are characterized, and the statistics are found to be well-described by random matrix theory predictions. The strength of spin-orbit scattering increases with atomic number and also varies between nanoparticles made of the same metal. The spin-orbit scattering rates in the nanoparticles are in order of magnitude agreement with bulk measurements on disordered samples.

PACS numbers: 73.22.-f, 72.25.Rb, 73.23.Hk

Spin-orbit (SO) interactions are central to determining the energy-level structure and dynamics of atomic nuclei, large-atomic-number atoms, and a wide variety of solid-state systems. They have important effects on electronic band structures [1], they influence the symmetry class of random-matrix theories applied to quantum systems [2], and they are put to use in proposals for controllable manipulation of electron spins [3]. A particularly fundamental method for probing SO interactions in solid-state systems is to examine individual quantum energy levels in nanoparticles, both because SO matrix elements can be measured directly and because SO interactions produce strong modifications of the effective g -factors for spin-Zeeman splitting. Previously, measurements of three individual energy levels in particular gold nanoparticles showed that SO effects reduce the g -factor to $g \sim 0.28 - 0.45$ [4], in sharp contrast with Al particles, which ordinarily give $g \approx 2$ [5]. Adding 4% gold to an aluminum nanoparticle also increased the SO scattering, thereby reducing the g -factors in the particle to $g \sim 0.5 - 0.8$ [6]. In this paper we report systematic studies of SO effects in noble-metal nanoparticles covering a range of atomic number (Z) – copper, silver, and gold. We characterize the mesoscopic fluctuations, present within single particles, of the g -factors and SO matrix elements $\langle H_{so} \rangle$, and find that the statistics for the g -factors are well-described by recent predictions of random matrix theory (RMT) [7,8]. From the values of the g -factors and the mean energy-level spacing δ [9], we extract SO scattering rates for each material, and we find order of magnitude agreement with expectations based on weak localization and electron spin resonance measurements.

SO interactions cause the electronic energy levels in a metal grain to be not purely spin-up or spin-down, and as a consequence they reduce the g -factor for spin-Zeeman splitting below the free-electron value of 2. In low- Z nanoparticles for which SO scattering is sufficiently weak (with $\langle H_{so} \rangle \ll \delta$) perturbation theory can be used to calculate the g -factor for a given electronic state n [10]:

$$g_n = 2 \left(1 - 2 \sum_{m \neq n} \frac{|\langle \Psi_{m\downarrow} | H_{so} | \Psi_{n\uparrow} \rangle|^2}{(E_n - E_m)^2} \right). \quad (1)$$

Here the Ψ_m denote the unperturbed (pure-spin) single-electron eigenstates with energy E_m . It is expected that the SO matrix elements will vary between different pairs of unperturbed energy levels because they depend on the precise nature of the wavefunctions, which are chaotic and fluctuating [11]. The local energy level spacing will also vary. As a result, g_n should exhibit mesoscopic fluctuations for different levels, n . For heavier elements, perturbation theory ceases to be valid. However, for large SO-interaction strengths, Brouwer *et al.* and Matveev *et al.* have recently employed RMT to predict the statistical distribution $P(g)$ of g -factors in a nanoparticle [7,8]. In [7], the strength of SO interactions is tuned continuously, allowing numerical studies of the full crossover from the Gaussian orthogonal ensemble (GOE) to the Gaussian symplectic ensemble (GSE) for the energy-level statistics. In this crossover, it is found that the mean value of $P(g)$ shifts to smaller g -factors and the variance of the distribution exhibits a maximum for $\langle g \rangle \sim 1.2$.

Our tunneling samples are fabricated in a vertical geometry through a 3–10 nm bowl-shaped hole etched in a Si_3N_4 membrane [5,12] (see inset, Fig. 1). One electrode is made by evaporating 1750 Å of Al on top of the membrane to fill the bowl. Following oxidation in 50 mTorr of O_2 for 3 minutes to form a tunnel barrier, 5–20 Å of Cu, Ag, or Au is evaporated on the lower side of the device to form particles with radii of 3–5 nm. A second tunnel barrier is then formed by the evaporation of 11 Å of Al_2O_3 . This is followed by 1750 Å of Al to make the lower tunneling electrode. The samples are screened at 4.2 K to select those whose current-voltage (I - V) curves exhibit Coulomb-staircase steps, indicating tunneling through a single nanoparticle. Then more detailed I - V curves are measured in a dilution refrigerator, with all electrical leads passing through copper-powder filters to minimize the effects of RF radiation.

Figure 1 shows I - V and dI/dV - V curves for a Cu

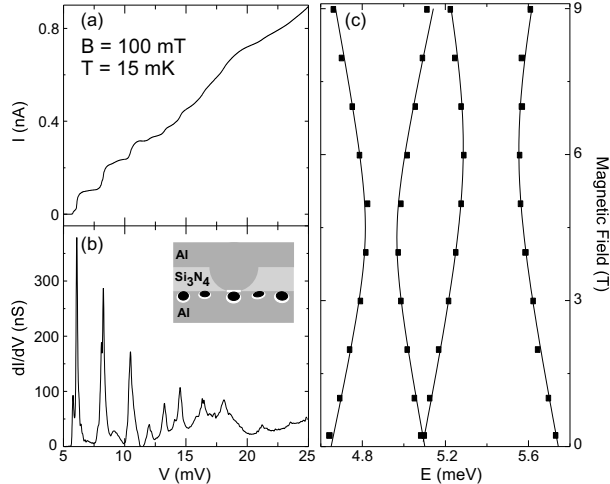


FIG. 1. (a) I - V and (b) dI/dV - V curves for Cu #1. (c) Magnetic field dependence of peaks in dI/dV for energy levels exhibiting avoided level crossings. The V scale has been converted to energy, using the procedure discussed in the text. Inset: Cross-sectional device schematic.

device (Cu#1). As V is increased, I increases in discrete steps due to tunneling through well-resolved energy levels within the nanoparticle [5]. The resonances in the differential conductance directly correspond to the energy level spectrum of the nanoparticle. In an applied magnetic field (H) most resonances in dI/dV divide into 2 peaks, allowing measurements of the energy-difference for spin-Zeeman splitting between Kramers-pair eigenstates, $\Delta E = g\mu_B H$. In order to determine the effective g -factors, we must convert the magnitude of the splitting from the measured value in voltage to energy, correcting for capacitive division of the voltage across the two tunnel junctions according to $\Delta E = \Delta V / (1 + C_1/C_2)$ where C_1/C_2 is the capacitance ratio for the two tunnel junctions. This ratio can be determined by measuring the shift in V for the resonances as the aluminum leads are changed from superconducting to normal in small magnetic fields, or by comparing the voltage for tunneling through the same quantum state for positive and negative V [5]. The low-field g -factors for sample Cu#1 fall in the range from 1.30 ± 0.04 to 1.82 ± 0.05 .

In the weak SO-scattering limit where perturbation theory is valid, the effects of SO interactions on the magnetic field evolution of neighboring energy levels (shown in detail in Fig. 1(c) and in broader view in Fig. 2(a)) can be modeled by diagonalizing a simple 2×2 Hamiltonian matrix with off-diagonal matrix elements $\langle H_{so} \rangle$ coupling the eigenstates [6]. The minimum energy difference at the avoided level crossing directly gives $2\langle H_{so} \rangle$ between those two states. The solid lines in Fig. 1(c) correspond to solutions of 2×2 Hamiltonians with $\langle H_{so} \rangle = 76 \mu\text{eV}$ for the avoided crossing near 4.9 meV, and $\langle H_{so} \rangle = 134 \mu\text{eV}$

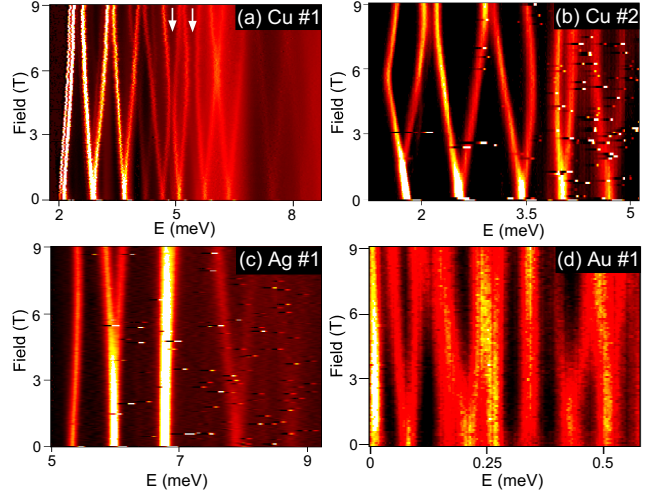


FIG. 2. Color scale plots of dI/dV in (a,b) Cu, (c) Ag, and (d) Au samples as a function of energy and magnetic field. The arrows denote the avoided crossings of Fig. 1.

for the avoided crossing near 5.4 meV. These matrix elements are in the size range expected based on the measured g -factors and the mean level spacing $\delta = 0.70$ meV. If the level spacing were uniform and equal to this value, and all the matrix elements $\langle H_{so} \rangle$ were $\sim 130 \mu\text{eV}$, then Eq. (1) would predict $g = 2 - 6.6(\langle H_{so} \rangle / \delta)^2 \sim 1.77$. If energy-level fluctuations are included, the estimate for the typical g -factor is somewhat smaller [8]. In accord with Eq. (1), we have seen that in a given sample the states which happen to have smaller-than-average energy spacings from neighboring levels generally have smaller-than-average g -factors.

For the heavier elements Ag and Au, the g -factors become smaller with increasing atomic number. Figure 2 shows color scale plots of dI/dV for increasing magnetic field in Cu, Ag, and Au samples. We find g -factors in the range 1.3 to 1.9 for Cu, 0.25 to 1.1 for Ag, and 0.05 to 0.19 in Au for the samples shown. Table 1 lists the measured mean values of the g -factors and their standard deviations for all the samples we have measured with more than three resolvable resonances.

The most direct way to compare the statistics of the measured g -factors with theoretical predictions is by plotting the integrated probability distribution of the g -factors for each sample. In Fig. 3 the points correspond to the g -factors from several Au, Ag, and Cu samples, while the solid lines are the theoretical predictions from Brouwer *et al.* [7] with the SO-scattering strength parameter λ adjusted to minimize the least squares error between the theoretical and experimental distributions. Our results are in good qualitative agreement with the RMT predictions. In particular, for a single value of the adjustable parameter λ , the theoretical distributions account reasonably for both the mean value of g and the

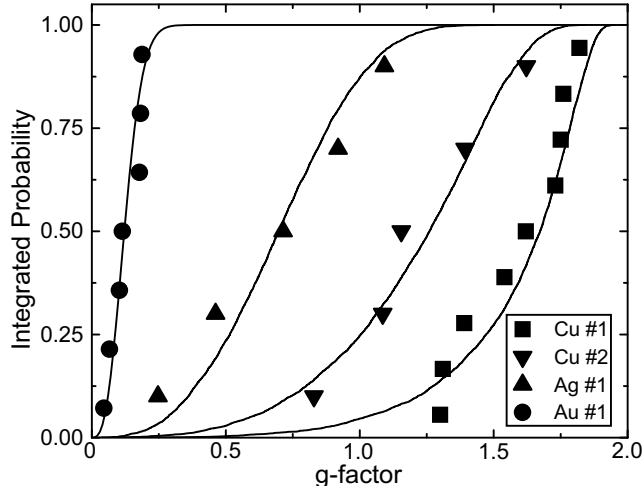


FIG. 3. Integrated probability distributions of the g -factors for several samples (points), compared to the predictions of random-matrix theory with the SO-interaction strength adjusted for the best fit (lines). See Table 1 for the sample parameters.

standard deviation for each sample.

We do observe significant differences in the average value of the g -factor for different nanoparticles composed of the same material, *e.g.*, for the two Cu samples depicted in Fig. 3 and for the Ag samples #1 and #2. This is true even though the mean level spacings for the two Cu samples are nearly identical. Because of these differences, we cannot meaningfully consolidate the data from many samples to improve the quality of our statistics in making comparisons to the RMT predictions. The physical origin of SO interactions at low temperatures within noble metal nanoparticles is expected to be scattering from defects or the nanoparticle surface [13–15]. Sample-to-sample variations in the strength of SO interactions are therefore reasonable in nanoparticles, if the defect concentration or the surface-to-volume ratio may vary, for instance due to size and shape differences between particles.

A few of the energy levels shown in Fig. 2 do not exhibit Zeeman splitting. We observe this only in samples where we can identify the tunneling transitions as corresponding to changes from an odd to an even number of conduction electrons within the particle. We make this identification by observing the lowest energy tunneling resonance. If the nanoparticle initially has an odd number of electrons, then the first energy level accessible for tunneling will have only one spin state available, and therefore the lowest energy transition does not undergo Zeeman splitting (Fig. 2(a,c,d)) [5]. In other words, the tunneling transition occurs via a spin-singlet state. Similarly, we can explain the lack of observed splitting in some higher energy resonances as due to tunneling via

excited spin-singlet states. (See the states near 7 meV in Fig. 2(c) and 0.3 meV in Fig. 2(d).) It is also possible that the Zeeman splitting may sometimes be sufficiently small for a level in Ag or Au that we cannot resolve it. Our resolution limit is approximately $g \geq 0.03$. From the theoretical probability distributions of Fig. 3, about 0.02% of the states in Ag and 1.4% of the states in Au can be expected to have $g < 0.03$.

In some samples, background-charge noise and nonequilibrium effects can interfere with accurate determinations of the statistics of the g -factors. For instance, as a function of the voltage across the device or as a function of time, the background charge affecting the nanoparticle can sometimes take on an ensemble of different values, shifting the energy levels that one is trying to measure. When this happens, current steps due to background-charge changes may be misinterpreted as due to quantum states, or the same quantum state may be measured several times at different values of voltage. In one Cu sample not shown in this paper, we measured six apparently different resonances all with an identical g -factor of 1.50, which we ascribe to this effect. This behavior was not seen in any other samples measured in this study. If several closely-spaced levels are observed in a sample, ways to diagnose the cause as background noise include the presence of negative differential conductance even with normal-state electrodes, the presence of apparent level crossings rather than avoided crossings, and identical g -factors for several resonance peaks.

An important question for understanding the properties of nm-scale devices is whether the strength of SO scattering is consistent with expectations based on measurements made by other techniques on larger samples, or whether there is new physics at small scales. Because effective g -factors measured by different experimental techniques can probe physically distinct quantities [8], we will make the comparison based on estimates for SO scattering times (τ_{so}) that we can extract from our data. We will also make comparison only to samples with mean free paths for electron scattering comparable to the size of our nanoparticles, since this scattering is the probable source of SO-induced spin relaxation [13,15]. In the limit of strong SO scattering in a nanoparticle, the relationship between the g -factor and τ_{so} has been solved analytically [8,9]:

$$\langle g^2 \rangle = \frac{3}{\pi\hbar} \tau_{\text{so}} \delta. \quad (2)$$

For the Au samples, using the values of δ listed in Table 1, we find $1/\tau_{\text{so}} = (2-8) \times 10^{12} \text{s}^{-1}$. The Ag and Cu samples fall outside the strong-scattering regime. However by fitting to the measured g -factors the numerical distributions calculated by Brouwer *et al.*, we can still determine τ_{so} for each sample from the single fitting parameter λ defined in [7]: $1/\tau_{\text{so}} = \lambda^2 \delta / (\pi\hbar)$. By this method, the SO scattering rates determined for the two Ag samples

are quite different, $1/\tau_{\text{so}} = 3 \times 10^{11} \text{s}^{-1}$ and $2 \times 10^{12} \text{s}^{-1}$, while for Cu $1/\tau_{\text{so}} = (2 - 8) \times 10^{11} \text{s}^{-1}$.

For Cu, we can also use perturbation theory to check the rate determined from the RMT approach. The value of τ_{so} within perturbation theory is [16]

$$1/\tau_{\text{so}} = \frac{2\pi|\langle H_{\text{so}} \rangle|^2}{\hbar\delta}. \quad (3)$$

For $\langle H_{\text{so}} \rangle \sim 130 \mu\text{eV}$ and $\delta=0.7 \text{ meV}$, we find $1/\tau_{\text{so}} \sim 2 \times 10^{11} \text{s}^{-1}$, in agreement with the rate for Cu#1 listed in Table 1.

These values for τ_{so} can be compared to the SO scattering rates measured previously by weak localization, and from the linewidths of conduction electron spin resonance (CESR) in metal foils. From weak localization measurements on quench-condensed noble-metal films, Bergmann [17] found $1/\tau_{\text{so}} = 5.4 \times 10^{12} \text{s}^{-1}$ for Au, $2.6\text{-}3.1 \times 10^{11} \text{s}^{-1}$ for Ag (depending on the disorder) and $3.2 \times 10^{11} \text{s}^{-1}$ for Cu. The values for Au and Cu agree to within a factor of three with all the rates we extract, while the weak-localization rate for Ag coincides with sample Ag#2 but not Ag#1. The CESR comparisons are less direct, because these measurements are performed on crystalline foils with thicknesses on the order of microns or more. In these experiments it is generally found that the spin-flip rate scales inversely with sample thickness due to the dominant effect of surface scattering [18]. The measured values include spin-flip rates of $7 \times 10^9 \text{s}^{-1}$ for Au foils one hundred microns thick [19], $1.5 \times 10^8 \text{s}^{-1}$ for a $5\text{-}\mu\text{m}$ -thick Ag foil [18], and $2.6 \times 10^8 \text{s}^{-1}$ for a $1.2 \mu\text{m}$ Cu film [20]. Assuming that the rates would scale as $1/\text{thickness}$ down to a thickness of 5 nm, we arrive at estimates of $1 \times 10^{14} \text{s}^{-1}$ for Au, $1 \times 10^{11} \text{s}^{-1}$ for Ag, and $6 \times 10^{10} \text{s}^{-1}$ for Cu. These SO scattering rates are also in rough order-of-magnitude agreement with the values obtained from the g -factor analysis.

In conclusion, we have measured the g -factor distributions in Cu, Ag, and Au nanoparticles using tunneling spectroscopy. The g -factors within a given sample exhibit mesoscopic fluctuations, with distributions in good accord with random-matrix-theory predictions. We have observed significant differences in both the g -factor distributions and τ_{so} between different nanoparticles composed of the same metal, illustrating the importance of the specific sample structure in the origin of SO scattering. The SO scattering rates we extract for the nanometer-scale particles are in rough order-of-magnitude agreement with extrapolations from previous CESR and weak localization measurements.

We thank Piet Brouwer and Xavier Waintal for discussions and the use of their simulation curves. This work was supported by the Packard Foundation and the NSF (DMR-0071631). JRP acknowledges the support of a NSF Graduate Research Fellowship. Sample fabrication was performed at the Cornell node of the National

-
- [1] N. W. Ashcroft and N. D. Mermin, *Solid State Physics* (Holt, Rinehart and Winston, Philadelphia, 1976).
 - [2] C. W. J. Beenakker, *Rev. Mod. Phys.* **69**, 731 (1997).
 - [3] S. Datta and B. Das, *Appl. Phys. Lett.* **56**, 665 (1990).
 - [4] D. Davidović and M. Tinkham, *Phys. Rev. Lett.* **83**, 1644 (1999).
 - [5] D. C. Ralph, C. T. Black, and M. Tinkham, *Phys. Rev. Lett.* **74**, 3241 (1995).
 - [6] D. G. Salinas, S. Gueron, D. C. Ralph, C. T. Black, and M. Tinkham, *Phys. Rev. B.* **60**, 6137 (1999).
 - [7] P. W. Brouwer, X. Waintal, and B. I. Halperin, *Phys. Rev. Lett.* **85**, 369 (2000).
 - [8] K. A. Matveev, L. I. Glazman, and A. I. Larkin, *Phys. Rev. Lett.* **85**, 2789 (2000).
 - [9] We define δ as the mean spacing between Kramers' doublets at $H=0$. This is the same definition used in [7], but it is twice the level spacing defined in [8].
 - [10] Sone, *J. Phys. Soc. Jpn.* **42**, 1457 (1977).
 - [11] M. L. Mehta, *Random Matrices* (Academic Press, San Diego, 1991).
 - [12] K. S. Ralls, R. A. Buhrman, and R. C. Tiberio, *Appl. Phys. Lett.* **55**, 2459 (1989).
 - [13] R. J. Elliott, *Phys. Rev.* **96**, 266 (1954).
 - [14] Y. Yafet, in *Solid State Physics*, edited by F. Seitz and D. Turnbull (Academic, New York, 1963), Vol. 14.
 - [15] For a recent review, see J. Fabian and S. Das Sarma, *J. Vac. Sci. Technol. B* **17**, 1708 (1999).
 - [16] W. P. Halperin, *Rev. Mod. Phys.* **58**, 533 (1986).
 - [17] G. Bergmann, *Z. Phys. B* **48**, 5 (1982).
 - [18] N. R. Couch, J. R. Sambles, A. Stesmans, and J. E. Cousins, *J. Phys. F: Met. Phys.* **12**, 2439 (1982).
 - [19] P. Monod and A. Janossy, *J. Low. Temp. Phys.* **26**, 311 (1977).
 - [20] A. Stesmans and J. R. Sambles, *J. Phys. F: Met. Phys.* **10**, L171 (1980).

TABLE I. Sample parameters. N is the number of resonances resolved, $\langle g \rangle$ is the mean g -factor, $\sigma_e(g)$ is the experimental standard deviation, $\sigma_t(g)$ is the standard deviation of the theory curve with the best-fit value of the SO parameter λ as defined in [7], δ is the mean level spacing, and $1/\tau_{\text{so}}$ is the spin-orbit scattering rate calculated as discussed in the text.

	N	$\langle g \rangle$	$\sigma_e(g)$	$\sigma_t(g)$	λ	$\delta(\text{meV})$	$1/\tau_{\text{so}}(\text{s}^{-1})$
Cu#1	9	1.58	0.20	0.17	0.7	0.70	2×10^{11}
Cu#2	5	1.22	0.30	0.31	1.2	0.71	5×10^{11}
Cu#3	5	0.79	0.29	0.29	2.1	0.36	8×10^{11}
Ag#1	5	0.69	0.34	0.27	2.4	0.85	2×10^{12}
Ag#2	5	1.54	0.07	0.17	0.7	1.13	3×10^{11}
Au#1	7	0.12	0.06	0.05	12.7	0.10	8×10^{12}
Au#2	7	0.17	0.07	0.07	9.5	0.12	5×10^{12}
Au#3	5	0.45	0.27	0.18	3.9	0.27	2×10^{12}